

# A Self-supervised Cascaded Refinement Network for Point Cloud Completion

Xiaogang Wang, *Student Member, IEEE*, Marcelo H Ang Jr, *Member, IEEE*, and Gim Hee Lee, *Member, IEEE*

**Abstract**—Point clouds are often sparse and incomplete, which imposes difficulties for real-world applications, such as 3D object classification, detection and segmentation. Existing shape completion methods tend to generate coarse shapes of objects without fine-grained details. Moreover, current approaches require fully-complete ground truth, which are difficult to obtain in real-world applications. In view of these, we propose a self-supervised object completion method, which optimizes the training procedure solely on the partial input without utilizing the fully-complete ground truth. In order to generate high-quality objects with detailed geometric structures, we propose a cascaded refinement network (CRN) with a coarse-to-fine strategy to synthesize the complete objects. Considering the local details of partial input together with the adversarial training, we are able to learn the complicated distributions of point clouds and generate the object details as realistic as possible. We verify our self-supervised method on both unsupervised and supervised experimental settings and show superior performances. Quantitative and qualitative experiments on different datasets demonstrate that our method achieves more realistic outputs compared to existing state-of-the-art approaches on the 3D point cloud completion task.



## 1 INTRODUCTION

**3D** point cloud has obtained an increasing attention in computer vision and deep learning due to its flexible representation and the popularity of various depth scanning devices. A large amount of works [1], [2], [3], [4] have been proposed for point cloud analysis by directly extracting pointwise features from the point coordinates. While they have achieved impressive results for 3D object classification or semantic segmentation, they are designed for complete and clean point sets, which performs inferior on sparse and incomplete 3D shapes, such as the raw data acquired by 3D sensors in self-driving cars and autonomous drones. Hence, shape completion is crucial for improving the perception abilities, such as object classification [5], detection [6], tracking [7], scene understanding [8], [9] and augmented reality [10], [11].

Existing methods [6], [12], [13], [14], [15], [16] have shown promising results on shape completion for different inputs, such as voxel grids, meshes and point clouds. Voxel representation is a direct generalization of pixels to the 3D case. While it is straightforward to adapt 2D convolutions to 3D for voxel generation [17], [18], the reconstruction process suffers from memory inefficiency, hence it is difficult to obtain high-resolution results. Although data-driven methods on mesh representations [19], [20], [21] show superiority on generating complicated surfaces, it is difficult to change the topology during the training process since they are limited to the fixed vertex connection patterns. In contrast, it is easy to add new points for point clouds and several studies have shown promising results. The pioneer work PCN [6] proposes an

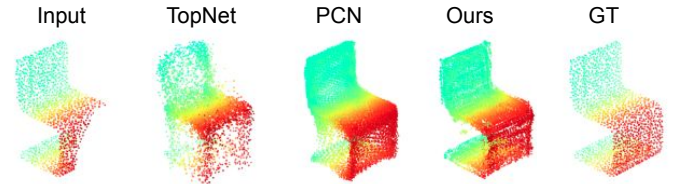


Fig. 1: Our method can generate complete point clouds with finer details compared to existing state-of-the-art methods.

encoder-decoder based architecture on both the synthetic dataset ShapeNet [22] and the real-world KITTI dataset [23]. Following work TopNet [12] proposes a hierarchical rooted tree-structure decoder to generate dense and complete objects. Although they have achieved impressive performances on different resolutions, they are unable to generate the detailed geometric structure of 3D objects. Several approaches [24], [25], [26] propose to learn 3D structures in a function space. They predict a binary classification score for each cell in a volumetric space to reconstruct surface boundaries by marchingcubes algorithm [27]. All the existing works are supervised learning approaches and require the fully-complete ground truth during training, which are not suitable for real-world applications.

In this work, we focus on the point cloud completion [6], [12] task and propose a self-supervised method, which is able to generate the object details at the same time. Figure 1 shows results between our method and existing approaches [6], [12]. Existing works failed to generate the lower part of the chair clearly, while ours result shows more accurate object shapes. We make a skip connection between the incomplete points and coarse outputs to preserve object details in the partial inputs. However, simple concatenation between inputs and our coarse outputs gives rise to unevenly distributed points. In order to alleviate this problem and generate missing parts with high quality, we design an iterative refinement decoder together with a feature contraction and expansion unit to refine the point positions. We adopt an adversarial loss

- X. Wang is with the Department of Mechanical Engineering, National University of Singapore, Singapore, 117575. E-mail: xiaogangw@u.nus.edu
- M. H. Ang, Jr. is with the Advanced Robotics Centre, Department of Mechanical Engineering, c, 117608. E-mail: mpeangh@nus.edu.sg
- G. H. Lee is with the Department of Computer Science, National University of Singapore, Computing 1, 13 Computing Drive, Singapore. E-mail: gimhee.lee@nus.edu.sg

Manuscript received August, 2020

to learn the complex point distributions and further improve the performance. The adversarial loss penalizes inaccurate points from the ground truth. Instead of predicting a single classification score like conventional generative adversarial networks (GANs) [17], [28], we adopt a patch-based discriminator to explicitly force every local patch of the generated point clouds to have the same pattern with ground truth point clouds inspired by [29], [30].

As to the self-supervised learning, we randomly resample a more incomplete object point cloud from the original partial object shape. We aim to mimic the standard shape completion procedure by correlating two different levels of partialness from the same object. This self-supervised strategy is a simple yet effective strategy for the shape completion problem. Although we have never seen the complete ground truth, we can still predict the missing parts with reasonable shapes. This randomly resampling operation can be implemented during the training process and is time-efficient. Furthermore, we propose a self-reconstruction strategy to reconstruct the partial input in parallel with the shape completion sub-network. We design an auto-encoder to reconstruct the partial inputs, in which encoder is shared with the completion sub-network and we only initialize the parameters of the decoder. By jointly training the auto-encoder with the completion pipeline, we can extract more accurate point features from the partial input, which is critical to generate high-fidelity 3D objects. We also adapt the MixUp strategy [31] from images to the point cloud completion inspired by [5]. A novel sample is created by the convex combination of two different object instances. Together with the resampling strategy and auto-encoder reconstruction method, MixUp yields large improvements over the state-of-the-art approaches for point cloud completion on both supervised and unsupervised experiments. We show state-of-the-art quantitative and qualitative results on different datasets by various experiments.

Our key contributions are as follows:

- We propose a novel point cloud completion network which is able to preserve object details from partial points and generate missing parts of high-quality at the same time;
- Our cascaded refinement strategy together with the coarse-to-fine pipeline can refine the point positions both locally and globally;
- We propose a self-supervised method on point cloud completion. Our proposed strategies can improve the performance on both the supervised and unsupervised learning;
- Our proposed self-supervised strategies can be incorporated into existing completion backbones seamlessly and improve their performances consistently;
- Experiments on different datasets show that our framework achieves superior results to existing methods on the 3D point cloud completion task.

## 2 RELATED WORKS

In this section, we review existing works on point cloud analysis and related works on shape completion.

### 2.1 Point Cloud Analysis

Point cloud learning has obtained increasing attention these years and a large amount of works have been proposed for the feature learning and down-stream tasks like classification,

segmentation and tracking. Currently, point cloud analysis methods can be roughly categorised into three directions [32]: point-wise Multi-Layer Perceptrons (MLP) based methods, convolution-based methods and graph-based methods.

**MLP-based Methods.** Pointwise MLP based methods extract each point features independently by several shared MLPs and then obtain the global object features via a symmetric function such as average-pooling or max-pooling. The pioneering work PointNet [1] extracts the pointwise features by several MLPs and then obtains the global embedding by a max-pooling operation. Although PointNet achieves impressive results on object classification and segmentation, they neglect the relationships among different points. Therefore, PointNet++ [2] proposes a hierarchical network to model the relationship geometric structures within the neighborhood by a set abstraction module. Inspired by PointNet and PointNet++, several works [33], [34], [35], [36] are proposed to consider the context of local neighborhood during the feature extraction.

**Convolution-based Methods.** Comparing with the pointwise MLPs, convolution based methods follow the conventional convolution mechanism in 2D image processing. In order to generalize typical CNNs to point clouds, PointCNN [37] proposes a  $\chi$ -transformation on the points to transform the unordered points into a potentially canonical order by MLPs. Then typical convolution can be used to extract point features. KPConv [38] defines a rigid and deformable kernel convolution on several kernel points. PointConv [39] proposes to use MLPs to approximate a weight function, and then calculates a density scale by a kernelized density estimation to re-weight the weights.

**Graph-based Methods.** Graph based approaches treat the points as vertexes and calculate the directed edges based on the nearby points. DGCNN [4] proposes a dynamic graph edge convolution on point clouds. The neighbors are selected dynamically based on the distances of different point features. Shen *et al.* [40] proposes a kernel correlation and graph pooling operation to consider the geometric affinities in the neighboring data points.

Among various point cloud analysis methods, PointNet [1] and PointNet++ [2] are widely used for point cloud generation and completion.

### 2.2 Point Cloud Completion

3D shape completion [14], [41], [42] plays an important role in robotics and perception, and has obtained significant development in recent years. Existing methods have shown impressive performances on various formats: voxel grids, meshes and point clouds. Inspired by 2D CNN operations, earlier works [14], [41], [43] focus on the voxel and distance fields formats generation with 3D convolution. Several approaches [14], [41] have proposed a 3D encoder-decoder based network for shape completion and shown promising performance. However, voxel based methods consume a large amount of memory and are unable to generate high-resolution outputs. To increase the resolution, several works [44], [45] have proposed to use the octree structure to gradually voxelize specific areas. However, due to the quantization effect of the voxelization operation, recent works gradually discard the voxel format and focus on the mesh reconstruction. Existing mesh representations [19], [46] are based on deforming a template mesh to a target mesh and hence not flexible to any typologies.

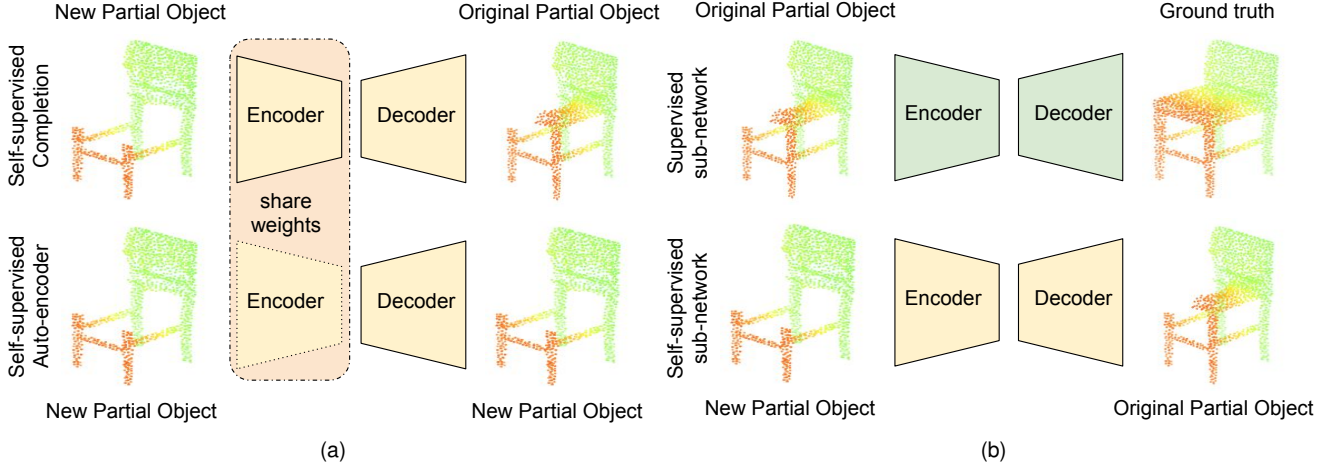


Fig. 2: The whole network of our self-supervised learning and a variant combined with the supervised optimization. (a) shows the self-supervised network architecture, which consists of two branches: the top branch represents for the completion pipeline and the bottom branch is the auto-encoder part. These two branches share the parameters of the encoder. The input and output for the completion branch are the more incomplete point cloud and the original partial object, while the input and output for the auto-encoder branch are the resampled more incomplete shapes. (b) shows the network for the joint learning between the self-supervised and supervised optimization. The upper part represents for the supervised learning with the original partial inputs and the fully-complete ground truth; the lower part represents for the self-supervised learning in (a).

In comparison to voxels and meshes, point clouds are easy to add new points during the training procedure. Yuan *et al.* [6] propose the pioneering work PCN on point cloud completion, which is a simple encoder-decoder network to reconstruct dense and complete point set from an incomplete point cloud. They adopts the folding mechanism [47] to generate high resolution outputs (16384). TopNet [12] proposes a hierarchical tree-structure network to generate point cloud without assuming any specific topology for the input point set. However, both PCN and TopNet are unable to synthesize the fine-grained details of 3D objects.

While recent works [48], [49], [50], [51], [52] on point cloud completion have shown improved performances, they are still limited in supervised learning. MSN [52] proposes a similar conditional method with ours, however, they sample points from the combined points between a coarse output and the partial input, while we first sample a subset from the partial input and concatenate with the coarse output, which preserves more object details compared to MSN. SG-NN [53] proposes a self-supervised method on scene completion by removing several frames from a given scan sequence. Then self-supervision is formulated by correlating two levels of partial scans from the same input sequence. Unlike SG-NN, we remove object regions whose point coordinates are within a distance threshold with respect to a randomly sampled center point.

### 3 OUR METHOD

#### 3.1 Overview

Given the sparse and incomplete point set  $P = \{p_i\}_{i=1}^N$  of  $N$  points, the target is to generate a dense and complete point set  $Q = \{q_i\}_{i=1}^{u \times N}$  of  $u \times N$  points, in which  $u$  is the upsampling scalar. Our objectives are two folds: (1) we aim to train the network with a self-supervised manner. Our self-supervised fashion enables the learning purely on the partial input without utilizing the fully-complete ground truth. This is essential for many real

world applications where the raw data are always sparse and incomplete, and it is also difficult to obtain the complete points due to the physical limitations of the RGB-D sensor or LiDARs. (2) we aim to produce complete and high-resolution 3D objects from corrupted and low resolution point clouds. Specifically, we expect the outputs to fulfill three requirements: (1) preserve the fine details of the input point cloud  $P$ , (2) inpaint the missing parts with detailed geometric structures, and (3) generate evenly distributed points on object surfaces. In the following part, we indicate the point clouds without ground truth as unlabeled data, and the point sets with ground truth as labeled data.

#### 3.2 Self-supervised Strategies

To achieve self-supervised learning, we propose three strategies: (1) we randomly resample more incomplete object shapes given the original partial inputs. More specifically, we further remove a specific region from the input shape to create new training pairs between the more incomplete objects and the original partial ones; (2) we design an auto-encoder reconstruction on the original partial input, in which we share the encoder parameters with the main completion framework and only initialize the parameters of the decoder. This helps the encoder to learn more accurate local and global features from the partial points, which is able to guide the decoder to generate object details shown in the incomplete shapes; (3) in order to learn the complicated data distribution from the entire unlabeled data, we adapt MixUp strategy [31] from images to our 3D shape completion problem. We randomly sample a coefficient from a *Beta* distribution to fuse two different object instances into one merged shape, for both the original partial inputs and the sampled incomplete objects. The basic idea of MixUp is to generate new training pairs by a convex combination between two different training examples, which are verified to be effective for domain adaption [5] and semi-supervised learning [31], [54], [55]. Our whole pipeline is shown in Figure 2. Figure 2(a) shows the self-supervised network

architecture, which consists of two branches: the top branch represents for the completion pipeline and the bottom branch is the auto-encoder part. These two branches share the parameters of the encoder. The input and output for the completion branch are the more incomplete point cloud and the original partial object, while the input and output for the auto-encoder branch are the resampled more incomplete shapes. Figure 2(b) shows the network for the joint optimization between the self-supervised and supervised learning. The upper part represents for the supervised learning with the original partial inputs and the fully-complete ground truth; the lower part represents for the self-supervised learning in (a).

### 3.2.1 Resampling

We create the partial and complete training data following PF-Net [48], RL-GAN-Net [56] and KAPLAN [57], in which we sample complete point clouds from the object surfaces and obtain the incomplete object shapes by randomly selecting a view point as the center and removing the points within a threshold from the complete point sets. In our experiments we sample 2048 points for the complete point clouds and randomly remove 512 points to make partial inputs [48], [56], [57]. Following this manner, we continue to remove another quarter of points from the partial inputs as the more incomplete object shapes. This is time-efficient and implemented in the data pre-processing stage during training. For a given partial object, we can generate different kinds of more incomplete point clouds corresponding to different missing regions. By training on the newly created example pairs, our network learns to predict the missing parts and synthesize the dense and complete object shapes without seeing the fully-complete ground truth.

### 3.2.2 Auto-encoder

Although existing point completion works achieve impressive results on different kinds of categories, they obtain inferior performance on reconstructing fine-grained details, which makes the output less realistic compared to the ground truth. Apart from the skip connection between the partial input with the intermediate coarse output, we propose to design another sub-network on reconstructing the partial inputs by an auto-encoder. The intuition is that by optimizing the Chamfer Distance (CD) [58] on the partial reconstruction, the encoder can implicitly extract more accurate partial features, which is beneficial for the decoder to reconstruct high-quality object shapes.

### 3.2.3 MixUp

MixUp method [31] is proposed as an extension of data augmentation considering both the images and one-hot labels. Given two input images and corresponding labels, MixUp generates new training images and labels by the convex combination, *i.e.*,

$$\begin{aligned} I' &= \gamma I_1 + (1 - \gamma) I_2, \\ L' &= \gamma L_1 + (1 - \gamma) L_2, \end{aligned} \quad (1)$$

in which  $I$ ,  $L$  and  $\gamma$  represent the images, labels and a coefficient sampled from a *Beta* distribution with fixed parameters, respectively. In our experiments, we adapt the Point Cloud MixUp (PCM) [5] strategy from the classification task to our point completion task. We implement the MixUp methods on both partial and complete point clouds. More specially, given two point cloud  $P_1, P_2 \in R^{n \times 3}$ , we sample a coefficient value

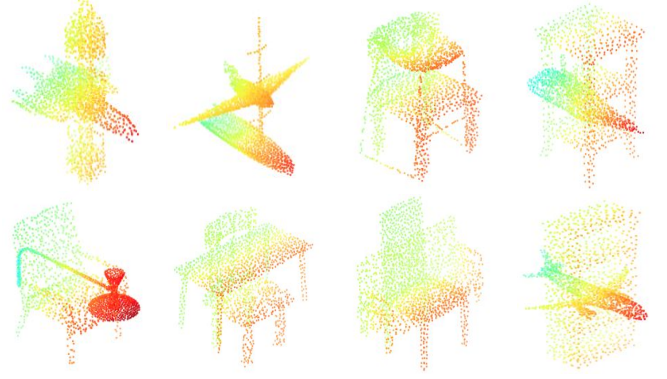


Fig. 3: Some point cloud examples of MixUp results.

$\gamma \in \text{Beta}(\alpha, \beta)$  and subsample two new sparser point clouds  $P'_1 \in R^{n_1}$ ,  $P'_2 \in R^{n_2}$  by the Farthest Point Sampling (FPS) [2], in which,

$$\begin{aligned} n_1 &= \gamma \times n, \\ n_2 &= (1 - \gamma) \times n. \end{aligned} \quad (2)$$

The coefficient  $\gamma$  is the same for the partial and complete point clouds. The mixed point sets are represented as the concatenation of  $P'_1$  and  $P'_2$ , *i.e.*  $[P'_1, P'_2]$ . Some merged examples are shown in Figure 3.

## 3.3 Cascaded Refinement Architecture

We design a novel cascaded refinement architecture to generate high-fidelity objects with fine-grained details. We adopt the adversarial training strategy to optimize the adversarial loss together with the reconstruction loss. The generator architecture is shown in Figure 4. Traditional GANs [59], [60], [61] map a noise distribution  $z$  to the data space, we extend the general GAN framework by modelling the generator  $G$  (Section 3.3.1) as a feature extraction encoder and a conditional coarse-to-fine decoder. The discriminator  $D$  (Section 3.3.4) aims to distinguish between the generated fake output and the ground truth.

### 3.3.1 Generator

Our generator  $G$  consists of three components: (1) feature extraction  $h$ , (2) coarse reconstruction  $g_1$  and (3) dense reconstruction  $g_2$ .

**Feature Extraction.** We use two stacked PointNet feature extraction architecture with max-pooling operation to extract the global point features  $f$  following PCN [6]. The feature extractor  $h$  consists of two functions, which are expressed as:

$$\begin{aligned} f &= h(P | w_h), \\ h &= h_1 \circ h_2, \end{aligned} \quad (3)$$

$h_1$  and  $h_2$  represent the two encoder sub-networks.  $w_h$  is the parameters of  $h_1$  and  $h_2$ .

**Coarse Reconstruction.**  $g_1$  includes several fully-connected layers mapping the latent embedding  $f$  to the coarse point cloud  $P_{\text{coarse}}$ . We denote the size of  $P_{\text{coarse}}$  as  $N_c \times 3$ . The coarse output roughly capture the complete object shape but loses fine details as shown in Figure 4. We aim to recover the object details in the dense reconstruction stage.



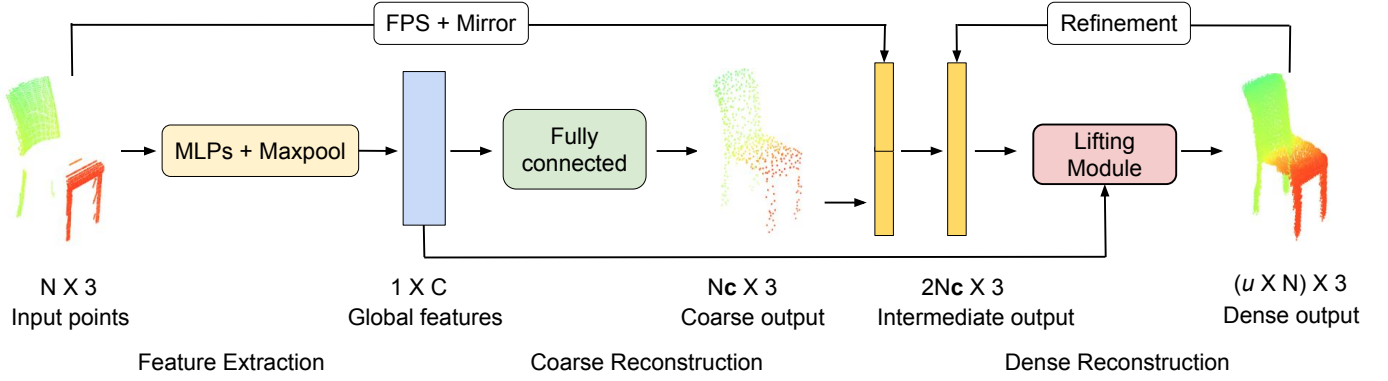


Fig. 4: An illustration of our generator network. The generator includes three sub-networks: feature extraction, coarse reconstruction and dense reconstruction. The feature extractor consists of two MLPs and max-pooling layers. The coarse reconstruction comprises several fully-connected layers. The dense reconstruction is a cascaded refinement sub-network with a lifting module in each step. We generate dense and complete point clouds given partial and sparse inputs.  $\mu$  is the upsampling factor.

**Dense Reconstruction.** Our second stage  $g_2$  is a conditional iterative refinement sub-network. The synthesis begins at generating low resolution points ( $2048 \times 3$ ), and points with higher resolutions are then progressively obtained. Our outputs have four resolutions:  $N = \{2048, 4096, 8192, 16384\}$  following TopNet [12], and the numbers of iterations are 1, 2, 3 and 4 for four resolutions. Parameters are shared among each iteration.

In order to generate dense and complete objects, existing methods [6], [12], [62] exploit either folding based operations or tree structure. Although they have achieved impressive qualitative results, the fine details of the objects are often lost. As can be seen in Figure 1, both PCN [6] and TopNet [12] fail to generate the details of 3D objects. The reason is that the latent embedding  $f$  is obtained by the last max-pooling layer of the encoder. It only represents the rough global shape, hence it is difficult to recover the detailed object structures. We propose to preserve the object details from the partial inputs and generate the missing parts with detailed structures from the global embedding  $f$  and  $P_{\text{coarse}}$  at the same time. We concatenate the partial inputs with the coarse output  $P_{\text{coarse}}$  inspired by the skip-connection from U-Net [63]. However, direct concatenation results in poor visual qualities because of the unevenly distributed points. To alleviate this problem, we propose to dynamically subsample  $N_c \times 3$  points from the partial inputs  $P$  before they are concatenated with the coarse output  $P_{\text{coarse}}$ . We denote the combined point sets as  $P_S$  with the size of  $2N_c \times 3$ , which are then fed into a lifting module (Section 3.3.2) to obtain a higher resolution points  $P_i$ . The point size is up-scaled by a factor of two via the lifting module. We use the FPS algorithm to subsample points. MSN [52] also proposes a similar conditional method with ours, however, we sample the partial inputs before the concatenation while MSN takes the opposite manner. We can preserve more partial details since some geometric structures maybe lost if sampling the combined point sets. We also design a feature contraction-expansion unit (Section 3.3.2) to gradually refine the point positions. For the subsequent iterates, the input for the lifting module is the intermediate output  $P_i$  from previous step.

### 3.3.2 Lifting Module

We design a lifting module to upsample the point size by a factor of two, and concurrently refine the point positions by the feature contraction-expansion unit. To upsample the point set  $P_S$ , we first

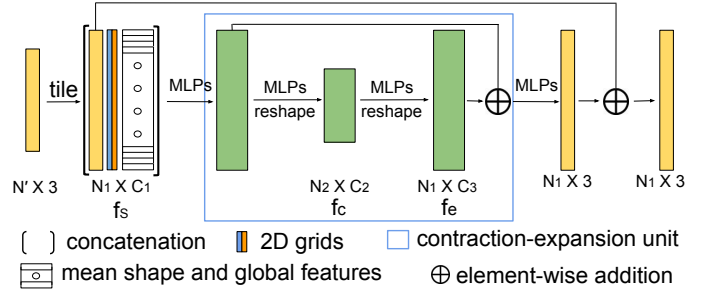


Fig. 5: The architecture of the lifting module. The input is  $N' \times 3$ , and we upsample it by a factor of 2 to obtain the output of  $N_1 \times 3$ . The feature contraction and expansion unit predicts residual point features instead of final results.

tile the points  $P_S$  two times to obtain a new point set  $P'_S$ . Then a unique 2D grid vector is sampled from a uniform distribution and is appended after each point coordinates to increase the variation among the duplicated points [47]. We also incorporate the mean shape prior  $f_m$  (Section 3.3.3) in our iterative refinement [64] to alleviate the domain gap of point features between the incomplete and complete point clouds. We concatenate the point  $P'_S$ , mean shape vectors  $f_m$ , global feature  $f$  and the sampled 2D grids to obtain a new feature  $f_s$ . Per-vertex displacements  $\{d_x, d_y, d_z\}$  are predicted for each point  $P'_S$  given the point feature  $f_s$  to obtain the dense and complete objects.

**Feature Contraction-expansion Unit.** Inspired by the hourglass network [65], we consolidate the local and global information by a bottom-up and top-down fashion to refine point positions and make them evenly distributed on object surfaces. Our lifting module is shown in Figure 5. We use shared multi-layer perceptrons (MLPs) [66] to make feature contraction and expansion due to its efficiency. More specifically, we assume the dimension of  $f_s$  to be  $N_1 \times C_1$ , and sizes of generated features  $f_c$  and  $f_e$  are  $N_2 \times C_2$  and  $N_1 \times C_3$ , respectively. The two operations are represented as  $f_c = \mathcal{RS}(\mathcal{C}_C(f_s))$  and  $f_e = \mathcal{RS}(\mathcal{C}_E(f_c))$ , where  $\mathcal{RS}(\cdot)$  is a reshaping operation.  $\mathcal{C}_C(\cdot)$  and  $\mathcal{C}_E(\cdot)$  are MLPs for contraction and expansion, respectively. Our lifting module predicts point feature residuals rather than the final output since deep neural networks are better at predicting residuals [19]. Overall, in one-

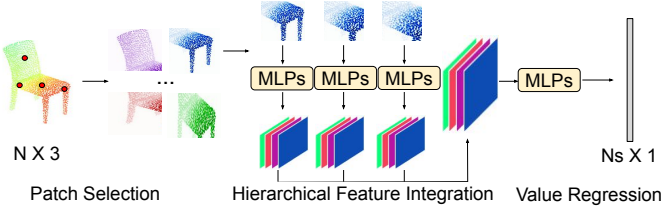


Fig. 6: The discriminator architecture sub-network. It includes the patch selection, hierarchical feature integration and confidence value regression.

step refinement, the output point set  $P_i$  is represented as:

$$P_i = F(P'_S) + P'_S, \quad (4)$$

where  $F(\cdot)$  predicts per-vertex offsets by the lifting module for the input point  $P'_S$ .

### 3.3.3 Shape Priors

We pre-train a PointNet auto-encoder<sup>1</sup> on all object categories following [64]. Object latent embeddings are obtained by a feeding the point clouds through the pre-trained encoder. For each object class, we take mean values of latent embeddings from all the instances within that category as our mean shape vectors. Similar to 3DN [21], we mirror the partial input with respect to the  $xy$ -plane as we assume the reflection symmetry plane ( $xy$ -plane) of objects to be known since many man-made models show global reflection symmetry. Therefore, a point set  $P_C$  with the size of  $N_c \times 3$  is obtained by mirroring the subsampled partial points.

### 3.3.4 Discriminator

To generate various realistic dense and complete point clouds, we adopt the adversarial training and jointly optimize the reconstruction loss and the adversarial loss end-to-end. The discriminator sub-network is shown in Figure 6. Our discriminator consists of patch selection, hierarchical feature integration and value regression. More architecture details are shown in supplementary materials.

## 3.4 Optimization

We take use of the Chamfer Distance (CD) [58] as our reconstruction loss. CD calculates the average closest point distance between two point clouds  $X$  and  $Y$ .

$$\begin{aligned} \text{CD}(X, Y) &= \mathcal{L}_{X,Y} + \mathcal{L}_{Y,X}, \text{ where} \\ \mathcal{L}_{X,Y} &= \frac{1}{|X|} \sum_{x \in X} \min_{y \in Y} \|x - y\|_2, \text{ and} \\ \mathcal{L}_{Y,X} &= \frac{1}{|Y|} \sum_{y \in Y} \min_{x \in X} \|x - y\|_2. \end{aligned} \quad (5)$$

Our training loss comprises two components, a reconstruction loss to encourage the completed point cloud to be the same as the ground truth, and an adversarial loss to penalize the unrealistic outputs.

**Reconstruction Loss.** There are two variants for CD which we denote as CD-1 and CD-2. Specifically, CD-2 takes the square root for the Euclidean distance and it is divided by 2. We adopt CD-2

in all our experiments during training, and evaluate with CD-1 and CD-2 in different datasets for fair comparison. We calculate both the CD losses for the coarse and fine outputs following the coarse-to-fine strategy [6]. Hence, our reconstruction loss can be expressed as:

$$\mathcal{L}_{\text{rec}} = \text{CD}(P_{\text{coarse}}, Y) + \lambda_f \text{CD}(P_{\text{fine}}, Y) + \lambda_{\text{ae}} \text{CD}(\hat{X}, X), \quad (6)$$

where  $P_{\text{coarse}}$ ,  $P_{\text{fine}}$  and  $\hat{X}$  represent the coarse output, fine output and the reconstructed partial point cloud, respectively.  $\lambda_f$  and  $\lambda_{\text{ae}}$  represent the weights for the CD of fine output and the reconstruction loss from the self-supervised auto-encoder, respectively.

**Adversarial Loss.** We adopt the stable and efficient objective function of LS-GAN [67] for our adversarial losses. Specifically, the adversarial losses for the generator and discriminator are:

$$\mathcal{L}_{\text{GAN}}(G) = \frac{1}{2} [D(\tilde{x}) - 1]^2, \quad (7)$$

$$\mathcal{L}_{\text{GAN}}(D) = \frac{1}{2} [D(\tilde{x})^2 + (D(x) - 1)^2], \quad (8)$$

where  $\tilde{x}$  and  $x$  are the generated fake result and the target ground truth, respectively.

**Overall Loss.** Our overall loss function is the weighted sum of the reconstruction loss and the adversarial losses:

$$\mathcal{L} = \lambda \mathcal{L}_{\text{GAN}} + \beta \mathcal{L}_{\text{rec}}, \quad (9)$$

where  $\lambda$  and  $\beta$  are the weights for GAN loss and the reconstruction loss, respectively. During training,  $G$  and  $D$  are optimized alternatively.

## 4 EXPERIMENTS

### 4.1 Evaluation Metrics

We compare our method with several existing methods 3D-EPN [14], PCN [6] and TopNet [12]. We use two evaluation metrics to evaluate results quantitatively. The first metric is CD following [6], [12]. More specifically, we use CD-2 for experiments in Section 4.4 and CD-1 in the remaining experiments. The other metric is Fréchet Point Cloud Distance (FPD) adopted from [62]. FPD calculates the 2-Wasserstein distance between the real and fake Gaussian measures in the feature spaces of the point sets:

$$\text{FPD}(X, Y) = \|\mathbf{m}_X - \mathbf{m}_Y\|_2^2 + \text{Tr}(\Sigma_X + \Sigma_Y - 2(\Sigma_X \Sigma_Y)^{\frac{1}{2}}), \quad (10)$$

where  $\mathbf{m}$  and  $\Sigma$  represent the mean vector and covariance matrix of the points, respectively.  $\text{Tr}(A)$  is the trace of matrix  $A$ .

### 4.2 Datasets

For a fair comparison, we first evaluate completion performance on the dataset of PCN [6]. The dataset of PCN has 30974 objects and eight categories selected from ShapeNet dataset [22]: airplane, cabinet, car, chair, lamp, sofa, table and vessel. The complete point clouds have 16384 points which are uniformly sampled from the mesh model. The incomplete point clouds have 2048 points. We also evaluate our method on another ShapeNet subset [5], [68] and ModelNet dataset [69] to verify the robustness of our method. These two datasets have ten categories: bathtub, bed, bookshelf, cabinet, chair, lamp, monitor, plant, sofa and table. We

1. <https://github.com/charlesq34/pointnet-autoencoder>

Methods	Mean Chamfer Distance per point ( $10^{-3}$ )								
	Avg	Airplane	Cabinet	Car	Chair	Lamp	Sofa	Table	Vessel
3D-EPN [14]	20.147	13.161	21.803	20.306	18.813	25.746	21.089	21.716	18.543
PCN-FC [6]	9.799	5.698	11.023	8.775	10.969	11.131	11.756	9.320	9.720
PCN [6]	9.636	5.502	10.625	8.696	10.998	11.339	11.676	8.590	9.665
TopNet [12]	9.890	6.235	11.628	9.833	11.498	9.366	12.347	9.362	8.851
CRN (CD-1)	8.868	5.065	10.383	8.650	9.830	9.830	11.002	8.253	8.335
CRN (CD-2)	<b>8.505</b>	<b>4.794</b>	<b>9.968</b>	<b>8.311</b>	<b>9.492</b>	<b>8.940</b>	<b>10.685</b>	<b>7.805</b>	<b>8.045</b>

TABLE 1: Quantitative comparison for point cloud completion on eight categories objects from PCN dataset.

assume the upright direction of all point clouds from different datasets are known and aligned. We rotate the upright direction of ModelNet from positive Z axis to positive Y axis to align with the ShapeNet datasets. ModelNet data contains 4183 training samples and 856 test samples and ShapeNet subset contains 17378 training samples and 2492 test samples. The ground truth point clouds are uniformly sampled from the object shapes by FPS. In order to further verify the effectiveness of our method, we also test on the real-world KITTI dataset [23].

### 4.3 Implementation Details

All our models are trained using the Adam [70] optimizer. We adopt the two time-scale update rule (TTUR) [71] and set learning rates for the generator and discriminator as 0.0001 and 0.00005, respectively. The learning rates are decayed by 0.7 after around every 40 epochs, and clipped by  $10^{-6}$  for the PCN dataset. There is no learning rate decay for the other two datasets.  $\lambda$ ,  $\lambda_{ae}$  and  $\beta$  are set to 1, 100 and 200, respectively.  $\lambda_f$  increases from 0.01 to 1 within the first 50000 iterations for the PCN dataset and is set to 1 for the other two datasets.  $N_s$  in discriminator is 256. The size  $N_c$  of coarse output is 512. We train one single model for all object categories. We denote CRN as the ‘‘cascaded refinement network’’ without self-supervised learning and ‘‘ours’’ as the whole network including CRN and self-supervised learning. The source code for CRN is available at <https://github.com/xiaogangw/cascaded-point-completion> for more implementation details. More experiments are in the supplementary materials.

### 4.4 Point Completion on the Dataset of PCN

Quantitative and qualitative results are shown in Table 1 and Figure 7. Point resolutions for the output and the ground truth are 16384. The quantitative results in Table 1 show that we obtain the best performance on all categories of objects compared to other methods. We obtain 11.7% relative improvement on the average value compared to the second best method PCN. This indicates that we achieve better performance with more accurate global shape and finer local structures. From Figure 7 we can observe that PCN and TopNet fail to recover the fine details such as legs of a chair and aircraft tails, while our method successfully generates such structures.

### 4.5 Point Completion on the ShapeNet and ModelNet

In this section, we test our method on the ShapeNet and ModelNet datasets [5], [68]. Quantitative and qualitative results are shown in Table 2 and Figure 8, respectively. As shown in Table 2, our method outperforms PCN and TopNet on almost all cases. The relative improvements of our method compared to PCN are

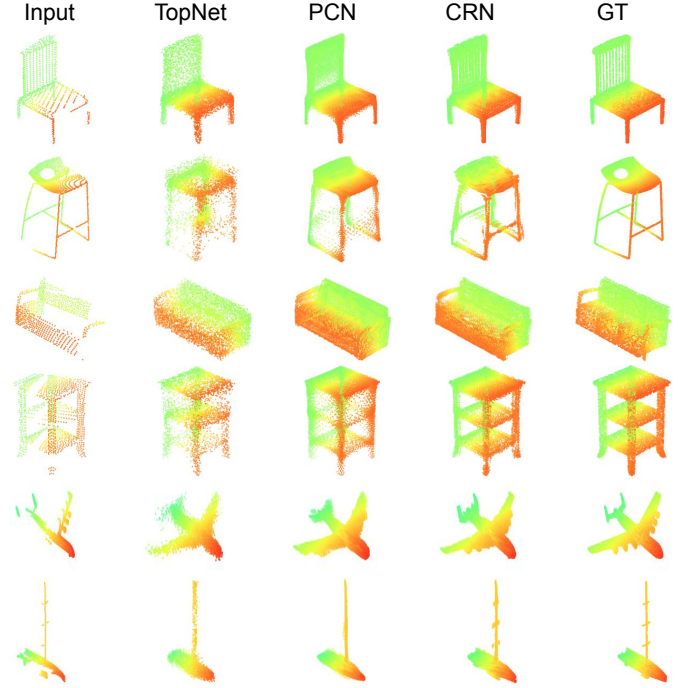


Fig. 7: Qualitative comparison on the dataset of PCN. Point resolutions for the output and ground truth are 16384.

26.3%, 24.5%, 23.7% and 24.4% for the ModelNet dataset on four resolutions, respectively. The improvements verify the robustness and generality of our method. Even though we obtain a little bit larger CD error on 16384 resolution results of the ShapeNet dataset compared to PCN, we achieve more reasonable qualitative results as shown in Figure 9. Our outputs capture more shape details although they are not distributed as uniformly as the results of PCN. This indicates that our method is able to generate more high-fidelity object shapes. The undistributed points can be alleviated by using the high resolution ground truth, which are easily sampled from the original mesh models, like the experiments on the dataset of PCN. We also generate 2048, 4096, 8192 and 16384 resolution objects by training one single model on 16384 points, and compare the results with that obtained from independent training of PCN and TopNet. We still achieve lower CD errors, which verifies the superiority of our method.

We obtain following conclusions from the qualitative results in Figure 8: (1) Our method is able to generate the details not only included in the partial scan, but also for the missing parts, on both high and low resolutions. For example, the legs of the tables and chairs. In contrast, both PCN and TopNet miss the detailed structure and only obtain the general object shapes. (2)



Resolution	ModelNet				ShapeNet			
	PCN [6]	TopNet [12]	CRN*	CRN	PCN [6]	TopNet [12]	CRN*	CRN
2048	3.537	4.171	2.896	<b>2.606</b>	3.091	3.550	2.786	<b>2.293</b>
4096	3.088	3.619	2.448	<b>2.332</b>	2.397	3.159	2.377	<b>2.086</b>
8192	2.778	2.818	2.128	<b>2.119</b>	1.981	2.838	2.117	<b>1.911</b>
16384	2.449	2.722	1.852	<b>1.852</b>	<b>1.754</b>	2.606	1.800	1.800

TABLE 2: Quantitative results on the ModelNet and ShapeNet datasets. We take CD ( $10^{-3}$ ) as evaluation results. Ours\* represents the results obtained by using the single model trained on the 16384 resolution output.

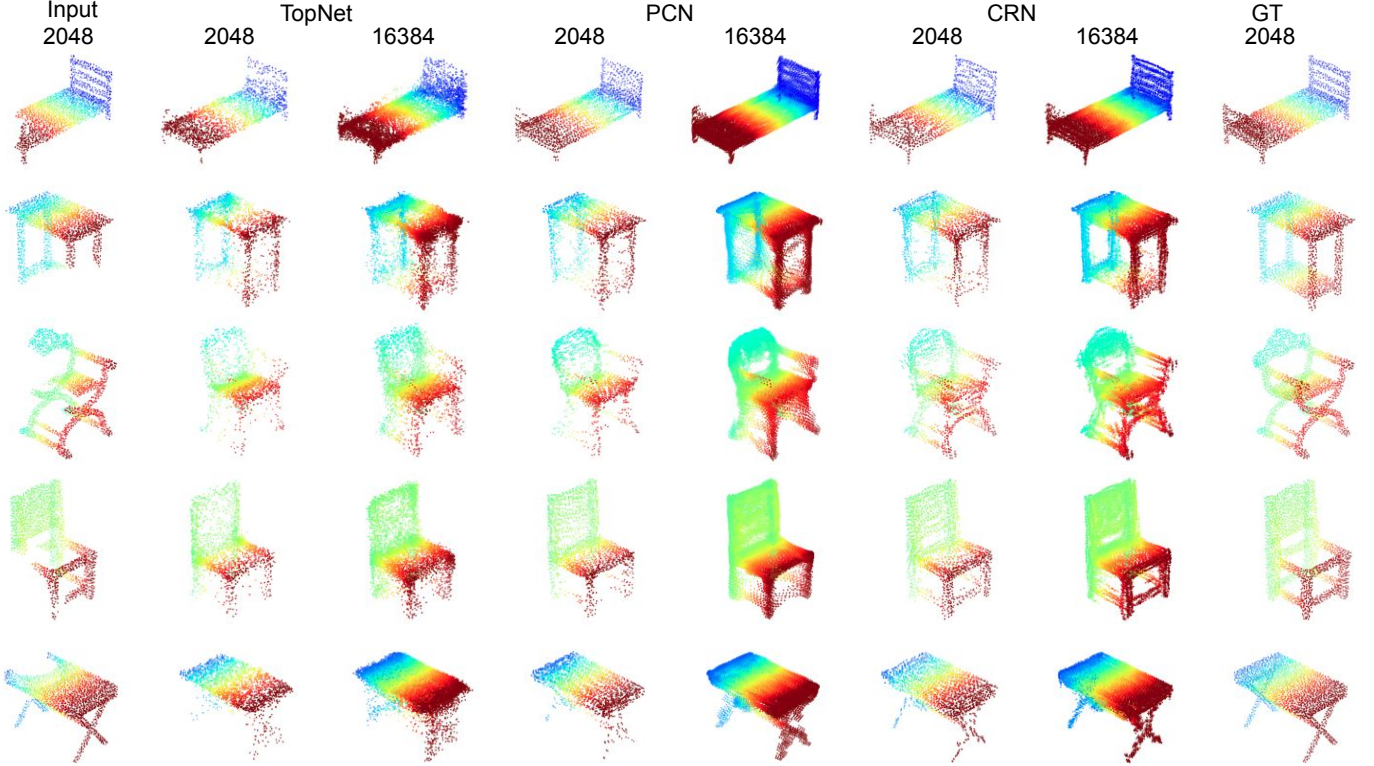


Fig. 8: Qualitative comparison on the ModelNet dataset. The resolution for both partial and ground truth are 2048. We show the generated results of size 2048 and 16384 from different methods.

Our generated points are more realistic. There are some points flying around the legs or arms of objects for the results of PCN and TopNet, while ours show clearer object outlines. More results are shown in our supplementary material.

#### 4.6 Point Completion for Occlusion Testing

To further test the robustness of the models, we manually occlude the partial inputs from the testing dataset of ModelNet and ShapeNet by  $p$  percent of points following PCN [6], and  $p$  ranges from 20% to 70% with a step of 10%. The quantitative results are shown in Table 3. Our method achieves the best performance for almost all the occlusion ratios, although the error increases gradually as more regions are occluded. This shows that our method is more robust to noisy data. More qualitative results are shown in our supplementary material.

#### 4.7 Ablation Study for CRN

We first evaluate the performances of different variants of CDs on the PCN dataset. The last two rows of Table 1 indicate that CD-2 achieves better results compared to CD-1, which indicates

that a sharper version of CD formulation benefits the training. Qualitative comparisons between CD-1 and CD-2 are shown in Figure 10. Although two different training losses both capture the general shapes with similar details of objects, the results of CD-2 are more evenly distributed compared to CD-1. For example, more points are clustered on the top corners of chairs from CD-1.

We also evaluate different components in our cascaded refinement network, including the adversarial training and the contraction-expansion unit. We denote our method without discriminator and contraction-expansion (CE) unit as the baseline (BS). The quantitative comparison are shown in Table 4. All experiments are done on the 2048 resolution points. We choose the bed category of ModelNet dataset as an example. We can see that our full pipeline performs the best. Removing any component decreases the performance, which verifies that each component contributes.

#### 4.8 Model Size Comparison

We evaluate the number of parameters in Table 5 for the resolution of 16384 points. We can see that our model has fewer parameters



Methods	ModelNet								ShapeNet							
	20%	30%	40%	50%	60%	70%	80%		20%	30%	40%	50%	60%	70%	80%	
PCN [6]	3.508	3.624	4.162	5.523	8.541	13.660	21.724		3.057	3.152	3.531	4.580	7.215	12.861	21.644	
TopNet [12]	2.654	2.762	<b>3.211</b>	4.451	7.516	12.985	21.264		2.567	2.679	3.052	4.046	6.585	14.391	35.400	
CRN	<b>2.538</b>	<b>2.747</b>	3.276	<b>4.431</b>	<b>7.189</b>	<b>12.285</b>	<b>19.378</b>		<b>2.272</b>	<b>2.360</b>	<b>2.704</b>	<b>3.694</b>	<b>6.005</b>	<b>10.691</b>	<b>18.104</b>	

TABLE 3: Quantitative comparison for occluded point clouds under different occlusion rates. The evaluation metric is mean CD per point ( $10^{-3}$ ).

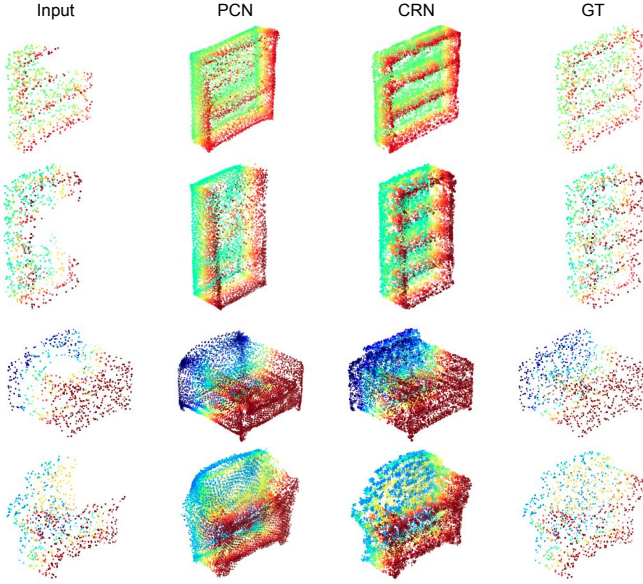


Fig. 9: Qualitative comparison on the ShapeNet dataset. The resolution of the output is 16384.

Method	BS	w/ CE	w/ GAN
CD ( $10^{-3}$ )	6.523	6.243	<b>6.181</b>

TABLE 4: Ablation studies on the bed category of the ModelNet dataset.

compared to PCN and TopNet, since we share the parameters in each cascaded refinement step.

Methods	PCN [6]	TopNet [12]	CRN
#Paras	6.85M	9.96M	<b>5.14M</b>

TABLE 5: Quantitative comparisons for model size.

#### 4.9 Unsupervised Experiments on the ModelNet and ShapeNet

In order to verify the effectiveness of our self-supervised learning. We first validate our approach on the unsupervised experiments, in which we treat all the training examples as unlabeled data. Thus, we train the neural network by optimizing CD-2 between the generated output from more incomplete point clouds and the original partial inputs, as well as the reconstruction loss of the partial objects. We make use of PCN and CRN as our two backbones and replace the training losses with our proposed self-supervised objectives. We denote the unsupervised training as “US”. We also train the fully-supervised PCN and CRN as the reference evaluations. Moreover, we further verify the effectiveness of our proposed self-supervised strategies by jointly training with the

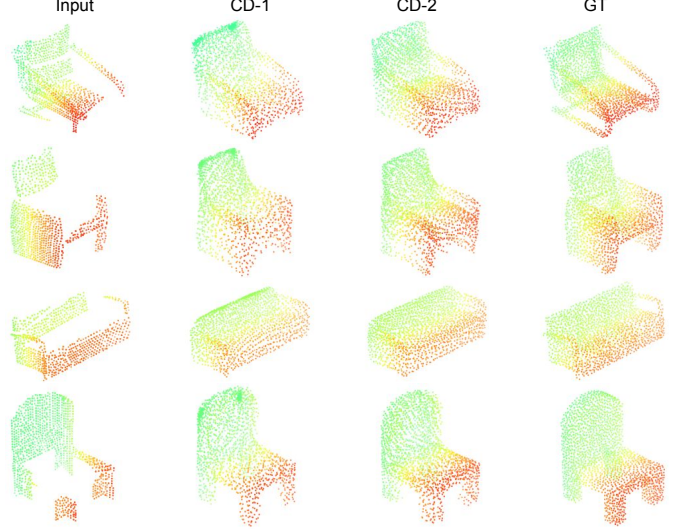


Fig. 10: Qualitative comparison between two variants of Chamfer Distance.

supervised backbones and denote them as “SS”. We first pre-train the backbone models and then optimize the supervised and unsupervised losses end-to-end for SS methods. The quantitative results of ModelNet is shown in Table 6. More results on the ShapeNet dataset are shown in the supplementary materials.

The first and fourth rows of Table 6 are the unsupervised results from PCN and CRN by optimizing our self-supervised objectives alone; the second and fifth rows are the standard supervised results by vanilla PCN and CRN; the third and sixth rows report the performances of joint optimization on both the unsupervised and supervised losses. We can obtain the following conclusions: (1): Our self-supervised approach is capable of completing the objects without accessing any fully complete point sets. Our unsupervised performances are comparable with the supervised results with PCN as the backbone, which indicates the effectiveness of our approach. (2): Comparison between the vanilla backbones and the SS methods indicates that our self-supervised strategies can further improve the performance of supervised approaches. When adding our self-supervised strategies to the PCN method, we decrease the CD error by a large margin of 20.2%, which demonstrates that our proposed methods successfully learn the accurate feature embeddings from the incomplete inputs and are able to generate high-fidelity object shapes. (3): Our methods are generalizable to different backbones. We further improve the supervised backbones consistently on different datasets by additionally optimizing with our proposed self-supervised techniques.

Qualitative comparison results on the ModelNet dataset by different methods are shown in Figure 11. The results are obtained by adopting PCN as the backbone. Three kinds of results are presented: unsupervised learning, standard supervised learning and

Methods	Mean Chamfer Distance per point ( $10^{-3}$ )										
	Avg	bathtub	bed	bookshelf	cabinet	chair	lamp	monitor	plant	sofa	table
PCN+US	3.733	3.885	3.608	3.768	4.480	2.859	5.217	3.188	5.629	3.637	2.424
PCN	3.541	2.886	2.192	3.325	3.427	2.416	15.058	2.405	8.149	2.439	1.987
PCN+SS	2.826	2.542	1.921	2.862	2.935	2.034	7.475	2.145	6.135	2.139	1.662
CRN+US	3.491	3.997	3.120	3.056	4.194	2.356	4.796	3.433	5.352	3.645	2.358
CRN	2.606	2.329	1.747	2.311	2.828	1.618	8.258	2.120	5.394	2.104	1.766
CRN+SS	2.472	2.409	1.717	2.258	2.804	1.607	6.133	2.121	4.862	2.112	1.645

TABLE 6: Quantitative comparison for point cloud completion on ten categories objects of ModelNet. US and SS represent the unsupervised and supervised methods with our self-supervised strategies, respectively.

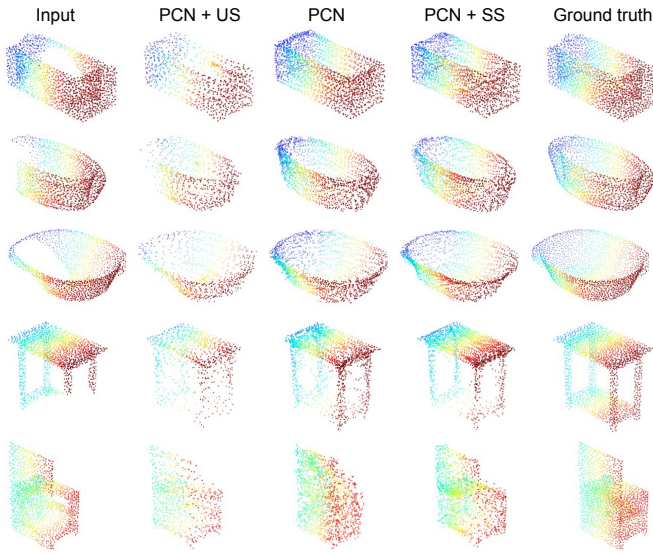


Fig. 11: Qualitative comparison results on the ModelNet dataset by different methods. US and SS represent the unsupervised and supervised methods with our self-supervised strategies, respectively.

joint optimization. We can obtain two conclusions: (1): Comparing between the PCN + US and PCN, we can see that even though some object details are missing, the unsupervised approach is capable of predicting the reasonable objects with general shapes. The missing parts of the inputs are also successfully completed. This verifies that the self-supervised strategies achieve the basic shape completion ability and work well on different objects. (2): Compared to the results from PCN baseline, fine-grained details together with more evenly distributed points are generated by the joint training with our proposed strategies. From the third row of Figure 11, we can see that points of PCN + SS have a more uniform distribution on the bowl surface compared to the other two methods. Moreover, the table and chair of row 4 and 5 from PCN + SS show cleaner object outlines compared with the other two methods, which indicate the superiority of our self-supervised approaches.

#### 4.10 Semi-supervised Experiments on the ModelNet and ShapeNet

By drawing varying ratios of labeled data out of the entire training set, we first pre-train the backbones with the labeled data samples in a fully-supervised way, then jointly optimize the supervised and self-supervised objectives with the labeled and remaining unlabeled data end-to-end.

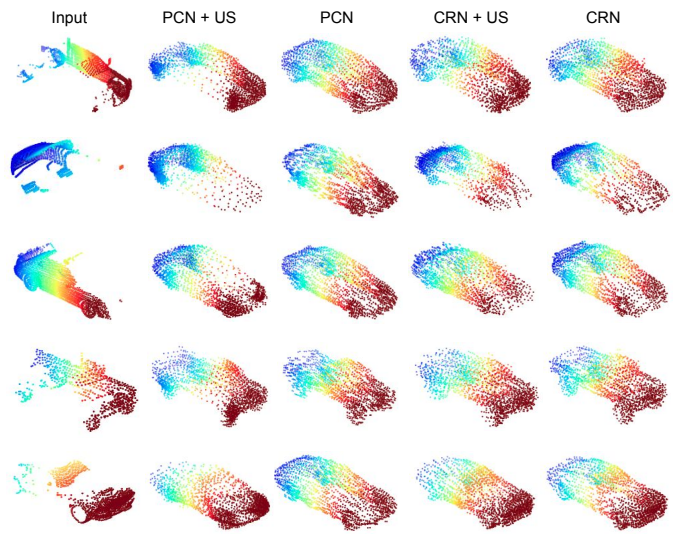


Fig. 12: Qualitative results on the KITTI dataset.

Table 7 lists the comparing results against supervised backbones under different ratios of labeled data on the ShapeNet and ModelNet datasets. By optimizing with the self-supervised strategies, the results significantly outperform the backbones. The improvements verify the effectiveness of our proposed self-supervised approaches. For both the ModelNet and ShapeNet, with the ratio of labeled data decrease, the margin between our method and the fully-supervised methods increase. Given 10% labeled data, our self-supervised strategies improve around 31.0% and 29.9% over PCN on the ModelNet and ShapeNet dataset, 16.7% and 12.0% over CRN on the ModelNet and ShapeNet dataset, respectively. This indicates that our self-supervised methods successfully learned knowledge from unlabeled data, and the benefits are larger when the number of available labeled data is smaller.

Furthermore, it is interesting that by using only 30% of labeled point clouds, training with self-supervision achieves close to the upper bound results which are obtained under the training with all labeled point clouds on the ModelNet dataset with PCN backbone. We attribute the out-performance of our self-supervision is capable of guiding the encoder sub-network to learn both the geometric and semantic information from the incomplete point clouds, which further helps the decoder to reconstruct object shapes with finer details. This indicates that our self-supervision strategies are complementary to supervised losses, and our framework can be integrated with other fully supervised point cloud completion pipelines.

Methods	ModelNet dataset					ShapeNet dataset				
	10%	30%	50%	70%	90%	10%	30%	50%	70%	90%
PCN	6.520	4.923	4.280	3.942	3.661	5.040	3.880	3.515	3.292	3.159
PCN-US <sup>†</sup>	<b>4.496</b>	<b>3.375</b>	<b>3.028</b>	<b>2.837</b>	<b>2.829</b>	<b>3.535</b>	<b>2.975</b>	<b>2.813</b>	<b>2.741</b>	<b>2.708</b>
Improv.(%)	31.0	31.4	29.3	28.0	22.7	29.9	23.3	20.0	16.7	14.3
CRN	4.291	3.413	2.981	2.803	2.669	3.226	2.706	2.524	2.411	2.341
CRN-US <sup>†</sup>	<b>3.574</b>	<b>2.816</b>	<b>2.600</b>	<b>2.494</b>	<b>2.433</b>	<b>2.840</b>	<b>2.491</b>	<b>2.412</b>	<b>2.310</b>	<b>2.305</b>
Improv.(%)	16.7	17.5	12.8	11.0	8.8	12.0	7.9	4.4	4.2	1.5

TABLE 7: Quantitative semi-supervised comparison for point cloud completion on ten categories objects of ModelNet and ShapeNet. Results are represented by mean Chamfer Distance per point ( $10^{-3}$ ). <sup>†</sup> represents the training with both labeled and unlabeled data. Labeled data are optimized with conventional completion losses, while unlabeled data are optimized with our self-supervised losses.

#### 4.11 Unsupervised Experiments on KITTI

Instead of testing on the synthetic datasets alone, we test on the real-world KITTI [23] dataset as well to show the robustness of our methods. We take a sequence of Velodyne scans from the KITTI dataset following PCN to obtain 2401 partial point clouds. Since existing methods cannot train on the KITTI dataset due to the lackness of corresponding ground truth, we train PCN and CRN on the car category of the ShapeNet dataset, then directly test on the KITTI dataset. As a comparison, we train another fully-unsupervised PCN and CRN by our self-supervised losses. The qualitative results are shown in Figure 12. The average number of points in the KITTI dataset is 440, in some cases even fewer than 10 points, which is much smaller compared to the average number of the synthetic ShapeNet dataset (larger than 1000). In spite of that, we obtain good results by optimizing the self-supervised losses compared with the supervised training (comparisons between the last two columns). The results of unsupervised PCN (second column) show inferior geometric structures compared to the results of our proposed CRN architecture (fourth column), which verifies that our cascaded refinement framework is able to extract the accurate point features and reconstruct high-fidelity object shapes, for both supervised and unsupervised training.

#### 4.12 Ablation Study for Self-supervised Learning

We explore the effects of three self-supervised strategies in this section. The training of ablation experiments is conducted on the ModelNet and ShapeNet with 10% labeled data. The evaluation is on the corresponding testing dataset. The output resolution is 2048. The results are shown in Table 8.

Resampling	Mixup	auto-encoder	ModelNet	ShapeNet
✗	✗	✗	6.887	5.040
✗	✗	✓	6.577	4.476
✗	✓	✗	6.050	4.457
✓	✗	✗	4.838	3.959
✓	✓	✓	<b>4.496</b>	<b>3.535</b>

TABLE 8: Ablation studies on the ModelNet and ShapeNet datasets. The results are obtained by adopting PCN as the network backbone. Results are represented by mean Chamfer Distance per point ( $10^{-3}$ ).

**Resampling.** We study the effect of resampling strategy by adding it on the backbones, and report the performances on the two datasets. It is obvious that we improve the performances significantly. This indicates the effectiveness of the proposed resampling strategy.

**MixUp.** We further investigate the effect of MixUp in our shape completion experiments. The improved results on the two datasets indicate the superiority of adapting the MixUp approach to the point cloud completion problem.

**Auto-encoding Reconstruction.** We verify the efficacy of auto-encoder sub-network during the completion process. Compared with the baseline method, CD are decreased on both the two datasets, which demonstrate that fewer errors are obtained by optimizing the reconstruction loss on the partial objects. Together with the other two methods, we achieve the best performance by using the three techniques.

## 5 CONCLUSION

In this work, we propose a self-supervised cascaded refinement network to generate complete points given the partial inputs. In order to synthesize the object details, our cascaded refinement generator exploits the existing details of the partial input points and synthesize the missing parts with high quality. We design a patch discriminator that leverages on adversarial training to learn the accurate point distribution and penalize the generated objects from infidelity to the ground truth. To mitigate the problem of supervised training, we propose three strategies to generate the complete objects without the fully-complete ground truth. Our self-supervised techniques are able to boost the performances for different backbones on both unsupervised and supervised learning. We evaluate our proposed method on different completion datasets. Various experiments show that our method achieves state-of-the-art performances.

## ACKNOWLEDGMENTS

This research was supported in part by the Singapore Ministry of Education (MOE) Tier 1 grant R-252-000-A65-114, National University of Singapore Scholarship Funds, the National Research Foundation, Prime Ministers Office, Singapore, under its CREATE programme, Singapore-MIT Alliance for Research and Technology (SMART) Future Urban Mobility (FM) IRG, and the Singapore Agency for Science, Technology and Research (A\*STAR) under its AME Programmatic Funding Scheme (Project #A18A2b0046).

## REFERENCES

- [1] C. R. Qi, H. Su, K. Mo, and L. J. Guibas, “Pointnet: Deep learning on point sets for 3d classification and segmentation,” in *Proceedings of the IEEE Conference on Computer Vision and Pattern Recognition*, 2017, pp. 652–660.

- [2] C. R. Qi, L. Yi, H. Su, and L. J. Guibas, "Pointnet++: Deep hierarchical feature learning on point sets in a metric space," in *Advances in Neural Information Processing Systems*, 2017, pp. 5099–5108.
- [3] J. Li, B. M. Chen, and G. Hee Lee, "So-net: Self-organizing network for point cloud analysis," in *Proceedings of the IEEE conference on computer vision and pattern recognition*, 2018, pp. 9397–9406.
- [4] Y. Wang, Y. Sun, Z. Liu, S. E. Sarma, M. M. Bronstein, and J. M. Solomon, "Dynamic graph cnn for learning on point clouds," *ACM Transactions on Graphics (TOG)*, 2019.
- [5] I. Achituve, H. Maron, and G. Chechik, "Self-supervised learning for domain adaptation on point-clouds," *arXiv preprint arXiv:2003.12641*, 2020.
- [6] W. Yuan, T. Khot, D. Held, C. Mertz, and M. Hebert, "Pcn: Point completion network," in *2018 International Conference on 3D Vision. IEEE*, 2018, pp. 728–737.
- [7] S. Giancola, J. Zarzar, and B. Ghanem, "Leveraging shape completion for 3d siamese tracking," in *Proceedings of the IEEE Conference on Computer Vision and Pattern Recognition*, 2019, pp. 1359–1368.
- [8] H. Ji, A. Dai, and M. Nießner, "3d-sis: 3d semantic instance segmentation of rgb-d scans," in *Proc. Computer Vision and Pattern Recognition (CVPR)*, IEEE, 2019.
- [9] A. Dai, D. Ritchie, M. Bokeloh, S. Reed, J. Sturm, and M. Nießner, "Scancomplete: Large-scale scene completion and semantic segmentation for 3d scans," in *Proc. Computer Vision and Pattern Recognition (CVPR)*, IEEE, 2018.
- [10] A. C. Boud, D. J. Haniff, C. Baber, and S. Steiner, "Virtual reality and augmented reality as a training tool for assembly tasks," in *1999 IEEE International Conference on Information Visualization (Cat. No. PR00210)*. IEEE, 1999, pp. 32–36.
- [11] A. Webster, S. Feiner, B. MacIntyre, W. Massie, and T. Krueger, "Augmented reality in architectural construction, inspection and renovation," in *Proc. ASCE Third Congress on Computing in Civil Engineering*, vol. 1, 1996, p. 996.
- [12] L. P. Tchappmi, V. Kosaraju, S. H. Rezatofighi, I. Reid, and S. Savarese, "Topnet: Structural point cloud decoder," in *The IEEE Conference on Computer Vision and Pattern Recognition (CVPR)*, 2019.
- [13] A. Brock, T. Lim, J. M. Ritchie, and N. Weston, "Generative and discriminative voxel modeling with convolutional neural networks," *arXiv preprint arXiv:1608.04236*, 2016.
- [14] A. Dai, C. Ruizhongtai Qi, and M. Nießner, "Shape completion using 3d-encoder-predictor cnns and shape synthesis," in *Proceedings of the IEEE Conference on Computer Vision and Pattern Recognition*, 2017, pp. 5868–5877.
- [15] O. Litany, A. Bronstein, M. Bronstein, and A. Makadia, "Deformable shape completion with graph convolutional autoencoders," in *Proceedings of the IEEE Conference on Computer Vision and Pattern Recognition*, 2018, pp. 1886–1895.
- [16] A. Sinha, A. Unmesh, Q. Huang, and K. Ramani, "Surfnet: Generating 3d shape surfaces using deep residual networks," in *Proceedings of the IEEE conference on computer vision and pattern recognition*, 2017, pp. 6040–6049.
- [17] J. Wu, C. Zhang, T. Xue, B. Freeman, and J. Tenenbaum, "Learning a probabilistic latent space of object shapes via 3d generative-adversarial modeling," in *Advances in neural information processing systems*, 2016, pp. 82–90.
- [18] E. Smith and D. Meger, "Improved adversarial systems for 3d object generation and reconstruction," *arXiv preprint arXiv:1707.09557*, 2017.
- [19] N. Wang, Y. Zhang, Z. Li, Y. Fu, W. Liu, and Y.-G. Jiang, "Pixel2mesh: Generating 3d mesh models from single rgb images," in *Proceedings of the European Conference on Computer Vision (ECCV)*, 2018, pp. 52–67.
- [20] T. Groueix, M. Fisher, V. G. Kim, B. C. Russell, and M. Aubry, "A papier-mâché approach to learning 3d surface generation," in *Proceedings of the IEEE conference on computer vision and pattern recognition*, 2018, pp. 216–224.
- [21] W. Wang, D. Ceylan, R. Mech, and U. Neumann, "3dn: 3d deformation network," in *Proceedings of the IEEE Conference on Computer Vision and Pattern Recognition*, 2019, pp. 1038–1046.
- [22] A. X. Chang, T. Funkhouser, L. Guibas, P. Hanrahan, Q. Huang, Z. Li, S. Savarese, M. Savva, S. Song, H. Su et al., "Shapenet: An information-rich 3d model repository," *arXiv preprint arXiv:1512.03012*, 2015.
- [23] A. Geiger, P. Lenz, C. Stiller, and R. Urtasun, "Vision meets robotics: The kitti dataset," *The International Journal of Robotics Research*, vol. 32, no. 11, pp. 1231–1237, 2013.
- [24] L. Mescheder, M. Oechsle, M. Niemeyer, S. Nowozin, and A. Geiger, "Occupancy networks: Learning 3d reconstruction in function space," in *Proceedings of the IEEE Conference on Computer Vision and Pattern Recognition*, 2019, pp. 4460–4470.
- [25] J. J. Park, P. Florence, J. Straub, R. Newcombe, and S. Lovegrove, "Deepsdf: Learning continuous signed distance functions for shape representation," in *Proceedings of the IEEE Conference on Computer Vision and Pattern Recognition*, 2019, pp. 165–174.
- [26] M. Michalkiewicz, J. K. Pontes, D. Jack, M. Baktashmotlagh, and A. Eriksson, "Deep level sets: Implicit surface representations for 3d shape inference," *arXiv preprint arXiv:1901.06802*, 2019.
- [27] M. Cubes, "A high resolution 3d surface construction algorithm," in *Proceedings of the 14th Annual Conference on Computer Graphics and Interactive Techniques*. New York: Association for Computing Machinery, 1987, pp. 163–69.
- [28] R. Li, X. Li, C.-W. Fu, D. Cohen-Or, and P.-A. Heng, "Pugan: a point cloud upsampling adversarial network," *arXiv preprint arXiv:1907.10844*, 2019.
- [29] P. Isola, J.-Y. Zhu, T. Zhou, and A. A. Efros, "Image-to-image translation with conditional adversarial networks," in *Proceedings of the IEEE conference on computer vision and pattern recognition*, 2017, pp. 1125–1134.
- [30] H. Wu, J. Zhang, and K. Huang, "Point cloud super resolution with adversarial residual graph networks," *arXiv preprint arXiv:1908.02111*, 2019.
- [31] H. Zhang, M. Cisse, Y. N. Dauphin, and D. Lopez-Paz, "mixup: Beyond empirical risk minimization," *arXiv preprint arXiv:1710.09412*, 2017.
- [32] Y. Guo, H. Wang, Q. Hu, H. Liu, L. Liu, and M. Bennamoun, "Deep learning for 3d point clouds: A survey," *IEEE Transactions on Pattern Analysis and Machine Intelligence*, 2020.
- [33] J. Yang, Q. Zhang, B. Ni, L. Li, J. Liu, M. Zhou, and Q. Tian, "Modeling point clouds with self-attention and gumbel subset sampling," in *Proceedings of the IEEE Conference on Computer Vision and Pattern Recognition*, 2019, pp. 3323–3332.
- [34] H. Zhao, L. Jiang, C.-W. Fu, and J. Jia, "Pointweb: Enhancing local neighborhood features for point cloud processing," in *Proceedings of the IEEE Conference on Computer Vision and Pattern Recognition*, 2019, pp. 5565–5573.
- [35] Y. Duan, Y. Zheng, J. Lu, J. Zhou, and Q. Tian, "Structural relational reasoning of point clouds," in *Proceedings of the IEEE Conference on Computer Vision and Pattern Recognition*, 2019, pp. 949–958.
- [36] X. Yan, C. Zheng, Z. Li, S. Wang, and S. Cui, "Pointasnl: Robust point clouds processing using nonlocal neural networks with adaptive sampling," in *Proceedings of the IEEE/CVF Conference on Computer Vision and Pattern Recognition*, 2020, pp. 5589–5598.
- [37] Y. Li, R. Bu, M. Sun, W. Wu, X. Di, and B. Chen, "Pointcnn: Convolution on x-transformed points," in *Advances in neural information processing systems*, 2018, pp. 820–830.
- [38] H. Thomas, C. R. Qi, J.-E. Deschaud, B. Marcotegui, F. Goulette, and L. J. Guibas, "Kpconv: Flexible and deformable convolution for point clouds," in *Proceedings of the IEEE International Conference on Computer Vision*, 2019, pp. 6411–6420.
- [39] W. Wu, Z. Qi, and L. Fuxin, "Pointconv: Deep convolutional networks on 3d point clouds," in *Proceedings of the IEEE Conference on Computer Vision and Pattern Recognition*, 2019, pp. 9621–9630.
- [40] Y. Shen, C. Feng, Y. Yang, and D. Tian, "Mining point cloud local structures by kernel correlation and graph pooling," in *Proceedings of the IEEE conference on computer vision and pattern recognition*, 2018, pp. 4548–4557.
- [41] X. Han, Z. Li, H. Huang, E. Kalogerakis, and Y. Yu, "High-resolution shape completion using deep neural networks for global structure and local geometry inference," in *Proceedings of the IEEE International Conference on Computer Vision*, 2017, pp. 85–93.
- [42] D. Stutz and A. Geiger, "Learning 3d shape completion from laser scan data with weak supervision," in *Proceedings of the IEEE Conference on Computer Vision and Pattern Recognition*, 2018, pp. 1955–1964.
- [43] T. Le and Y. Duan, "Pointgrid: A deep network for 3d shape understanding," in *Proceedings of the IEEE conference on computer vision and pattern recognition*, 2018, pp. 9204–9214.
- [44] P.-S. Wang, Y. Liu, Y.-X. Guo, C.-Y. Sun, and X. Tong, "O-cnn: Octree-based convolutional neural networks for 3d shape analysis," *ACM Transactions on Graphics (TOG)*, vol. 36, no. 4, p. 72, 2017.
- [45] P.-S. Wang, C.-Y. Sun, Y. Liu, and X. Tong, "Adaptive o-cnn: a patch-based deep representation of 3d shapes," in *SIGGRAPH Asia 2018 Technical Papers*. ACM, 2018, p. 217.
- [46] M. Vakalopoulou, G. Chassagnon, N. Bus, R. Marini, E. I. Zacharaki, M.-P. Revel, and N. Paragios, "Atlasnet: multi-atlas non-linear deep networks for medical image segmentation," in *International Conference on Medical Image Computing and Computer-Assisted Intervention*. Springer, 2018, pp. 658–666.



- [47] Y. Yang, C. Feng, Y. Shen, and D. Tian, "Foldingnet: Point cloud auto-encoder via deep grid deformation," in *Proceedings of the IEEE Conference on Computer Vision and Pattern Recognition*, 2018, pp. 206–215.
- [48] Z. Huang, Y. Yu, J. Xu, F. Ni, and X. Le, "Pf-net: Point fractal network for 3d point cloud completion," in *Proceedings of the IEEE/CVF Conference on Computer Vision and Pattern Recognition*, 2020, pp. 7662–7670.
- [49] W. Zhang, Q. Yan, and C. Xiao, "Detail preserved point cloud completion via separated feature aggregation," *arXiv preprint arXiv:2007.02374*, 2020.
- [50] X. Wen, T. Li, Z. Han, and Y.-S. Liu, "Point cloud completion by skip-attention network with hierarchical folding," in *Proceedings of the IEEE/CVF Conference on Computer Vision and Pattern Recognition*, 2020, pp. 1939–1948.
- [51] H. Xie, H. Yao, S. Zhou, J. Mao, S. Zhang, and W. Sun, "Grnet: Griding residual network for dense point cloud completion," in *ECCV*, 2020.
- [52] M. Liu, L. Sheng, S. Yang, J. Shao, and S.-M. Hu, "Morphing and sampling network for dense point cloud completion," *arXiv preprint arXiv:1912.00280*, 2019.
- [53] A. Dai, C. Diller, and M. Nießner, "Sg-nn: Sparse generative neural networks for self-supervised scene completion of rgb-d scans," in *Proceedings of the IEEE/CVF Conference on Computer Vision and Pattern Recognition*, 2020, pp. 849–858.
- [54] D. Berthelot, N. Carlini, I. Goodfellow, N. Papernot, A. Oliver, and C. A. Raffel, "Mixmatch: A holistic approach to semi-supervised learning," in *Advances in Neural Information Processing Systems*, 2019, pp. 5049–5059.
- [55] V. Verma, A. Lamb, C. Beckham, A. Najafi, I. Mitliagkas, D. Lopez-Paz, and Y. Bengio, "Manifold mixup: Better representations by interpolating hidden states," in *International Conference on Machine Learning*, 2019, pp. 6438–6447.
- [56] M. Sarmad, H. J. Lee, and Y. M. Kim, "Rl-gan-net: A reinforcement learning agent controlled gan network for real-time point cloud shape completion," in *Proceedings of the IEEE Conference on Computer Vision and Pattern Recognition*, 2019, pp. 5898–5907.
- [57] A. Richard, I. Cherabier, M. R. Oswald, M. Pollefeys, and K. Schindler, "Kaplan: A 3d point descriptor for shape completion," *arXiv preprint arXiv:2008.00096*, 2020.
- [58] H. Fan, H. Su, and L. J. Guibas, "A point set generation network for 3d object reconstruction from a single image," in *Proceedings of the IEEE conference on computer vision and pattern recognition*, 2017, pp. 605–613.
- [59] I. Goodfellow, J. Pouget-Abadie, M. Mirza, B. Xu, D. Warde-Farley, S. Ozair, A. Courville, and Y. Bengio, "Generative adversarial nets," in *Advances in Neural Information Processing Systems (NIPS)*, 2014.
- [60] P. Achlioptas, O. Diamanti, I. Mitliagkas, and L. Guibas, "Learning representations and generative models for 3D point clouds," in *Proceedings of the 35th International Conference on Machine Learning*. PMLR, 2018.
- [61] D. Valsesia, G. Fracastoro, and E. Magli, "Learning localized generative models for 3d point clouds via graph convolution," 2018.
- [62] D. W. Shu, S. W. Park, and J. Kwon, "3d point cloud generative adversarial network based on tree structured graph convolutions," *arXiv preprint arXiv:1905.06292*, 2019.
- [63] O. Ronneberger, P. Fischer, and T. Brox, "U-net: Convolutional networks for biomedical image segmentation," in *International Conference on Medical image computing and computer-assisted intervention*. Springer, 2015, pp. 234–241.
- [64] A. Kanazawa, M. J. Black, D. W. Jacobs, and J. Malik, "End-to-end recovery of human shape and pose," in *Proceedings of the IEEE Conference on Computer Vision and Pattern Recognition*, 2018, pp. 7122–7131.
- [65] A. Newell, K. Yang, and J. Deng, "Stacked hourglass networks for human pose estimation," in *European conference on computer vision*. Springer, 2016, pp. 483–499.
- [66] L. Yu, X. Li, C.-W. Fu, D. Cohen-Or, and P.-A. Heng, "Pu-net: Point cloud upsampling network," in *Proceedings of the IEEE Conference on Computer Vision and Pattern Recognition*, 2018, pp. 2790–2799.
- [67] X. Mao, Q. Li, H. Xie, R. Y. Lau, Z. Wang, and S. Paul Smolley, "Least squares generative adversarial networks," in *Proceedings of the IEEE International Conference on Computer Vision*, 2017, pp. 2794–2802.
- [68] C. Qin, H. You, L. Wang, C.-C. J. Kuo, and Y. Fu, "Pointdan: A multi-scale 3d domain adaption network for point cloud representation," in *Advances in Neural Information Processing Systems*, 2019, pp. 7192–7203.
- [69] Z. Wu, S. Song, A. Khosla, F. Yu, L. Zhang, X. Tang, and J. Xiao, "3d shapenets: A deep representation for volumetric shapes," in *Proceedings of the IEEE conference on computer vision and pattern recognition*, 2015, pp. 1912–1920.
- [70] D. P. Kingma and J. Ba, "Adam: A method for stochastic optimization," *arXiv preprint arXiv:1412.6980*, 2014.
- [71] M. Heusel, H. Ramsauer, T. Unterthiner, B. Nessler, and S. Hochreiter, "Gans trained by a two time-scale update rule converge to a local nash equilibrium," in *Advances in Neural Information Processing Systems*, 2017, pp. 6626–6637.



completion and visual relationship detection.



in 1986 and 1988, respectively. His work experience includes heading the Technical Training Division of Intel's Assembly and Test Facility in the Philippines, research positions at the East West Center in Hawaii and at the Massachusetts Institute of Technology, and a faculty position as an Assistant Professor of Electrical Engineering at the University of Rochester, New York. In 1989, Dr. Ang joined the Department of Mechanical Engineering of the National University of Singapore, where he is currently a Professor. He is also the Acting Director of the Advanced Robotics Centre. His research interests span the areas of robotics, mechatronics, and applications of intelligent systems methodologies. He teaches both at the graduate and undergraduate levels in the following areas: robotics; creativity and innovation, and Engineering Mathematics. He is also active in consulting work in robotics and intelligent systems. In addition to academic and research activities, he is actively involved in the Singapore Robotic Games as its founding chairman and the World Robot Olympiad as a member of the Advisory Council.



research interests include computer vision, robotic perception and machine learning. He serves as an Area Chair for BMVC 2020, 3DV 2020 and CVPR 2021, and will be part of the organizing committee as the Exhibition/Demo Chair for CVPR 2023.

**Xiaogang Wang** is a Ph.D student in the Department of Mechanical Engineering, National University of Singapore, supervised by Prof. Marcelo H Ang Jr and Prof. Gim Hee Lee. He obtained his M.Eng. degree in Mechanical Engineering from the Beihang University in 2016; and the B.Sc. degree in Mechanical Engineering from the University of Science and Technology Beijing in 2013, respectively. His research interests are computer vision and deep learning. Specific efforts have been made in 3D shape

**Marcelo H Ang Jr** is a Professor in the Department of Mechanical Engineering, National University of Singapore. He received the B.Sc. degrees (Cum Laude) in Mechanical Engineering and Industrial Management Engineering from the De La Salle University, Manila, Philippines, in 1981; the M.Sc. degree in Mechanical Engineering from the University of Hawaii at Manoa, Honolulu, Hawaii, in 1985; and the M.Sc. and Ph.D. degrees in Electrical Engineering from the University of Rochester, Rochester, New York, in 1986 and 1988, respectively. His work experience includes heading the Technical Training Division of Intel's Assembly and Test Facility in the Philippines, research positions at the East West Center in Hawaii and at the Massachusetts Institute of Technology, and a faculty position as an Assistant Professor of Electrical Engineering at the University of Rochester, New York. In 1989, Dr. Ang joined the Department of Mechanical Engineering of the National University of Singapore, where he is currently a Professor. He is also the Acting Director of the Advanced Robotics Centre. His research interests span the areas of robotics, mechatronics, and applications of intelligent systems methodologies. He teaches both at the graduate and undergraduate levels in the following areas: robotics; creativity and innovation, and Engineering Mathematics. He is also active in consulting work in robotics and intelligent systems. In addition to academic and research activities, he is actively involved in the Singapore Robotic Games as its founding chairman and the World Robot Olympiad as a member of the Advisory Council.

**Gim Hee Lee** is currently an Assistant Professor at the Department of Computer Science at the National University of Singapore (NUS), where he heads the Computer Vision and Robotic Perception (CVRP) Laboratory. He is also affiliated with the NUS Institute of Data Science. He was a researcher at Mitsubishi Electric Research Laboratories (MERL), USA. Prior to MERL, he did his PhD in Computer Science at ETH Zurich, and B.Eng with first class honors and M.Eng degrees in Mechanical Engineering at NUS. His